Received February 8, 2018, accepted March 31, 2018, date of publication April 12, 2018, date of current version June 20, 2018.

Digital Object Identifier 10.1109/ACCESS.2018.2826015

Load Frequency Control of a Novel Renewable Energy Integrated Micro-Grid Containing Pumped Hydropower Energy Storage

YANHE XU[1], CHAOSHUN LI[1], (Member, IEEE), ZANBIN WANG[1], NAN ZHANG[1], AND BING PENG[2]

[1]School of Hydropower and Information Engineering, Huazhong University of Science and Technology, Wuhan 430074, China
[2]China Yangtze Power Co., Ltd., Yichang 443000, China

Corresponding author: Chaoshun Li (csli@hust.edu.cn)

This work was supported by the National Natural Science Foundation of China under Grant 51679095 and Grant 51479076.

ABSTRACT In this paper, a novel energy storage method based on pumped hydropower energy storage (PHES) for a renewable energy integrated micro-grid (REMG) is proposed, and the load frequency control (LFC) for the system is studied. In a typical REMG, micro pumped storage units are built that rely on a tall building to convert energy by pumping water up to store energy and releasing the stored water to generate energy. Because of the fluctuation of renewable energy (RE) and the perturbation of the load demand, frequency deviation, and tie-line power interchange are inevitable. In this paper, the LFC controller optimization problem for the REMG is investigated, and the optimal controllers for multi-areas in the REMG are designed. To solve the optimization problem of LFC, a novel meta-heuristic algorithm called artificial sheep algorithm (ASA) is applied in the task of LFC optimization. In the experiments, RE scenarios of different seasons, the impact of PHES, and the control robustness are studied. The results not only prove the feasibility of the proposed REMG but also show the effectiveness of the optimized controllers in maintaining frequency stability under various conditions.

INDEX TERMS Renewable energy integrated micro-grid, micro pumped storage unit, load frequency control, artificial sheep algorithm, controller optimization.

I. INTRODUCTION

Nowadays, the increasing for energy and the depletion of fossil fuels have necessitated the large-scale utilization of RE [1]. RE sources, regarded as clean and economical energy sources, are likely to be connected to micro-grid power systems [2] for distributed utilization; the study of REMGs has become a popular topic in research and applications. In a REMG, the energy storage system (ESS) is one of the most critical components. The ESS is an indispensable part of a micro-grid, because the use of an ESS improves power quality and ensures the safe and reliable operation of micro-grids [3], [4]. The conventional ESSs applied in REMG is batteries [3], [5], flywheels [6] and so on. In [7], an ESS based on the idea of Vehicle-to-Grid (V2G) was proposed in which batteries of electric vehicles are considered as a distributed ESS in MGs. Compared with the popular ESSs mentioned above, PHES has proven to be one of the most effective large-scale ESSs for the power grid, showing striking advantages on capacity, cost and efficiency. In view of the performance of PHES as an ESS in a large power grid [8], an interesting question is posed: would a small/micro-scale PHES be an effective ESS for a REMG?

The goal of this paper is to design a REMG, in which the ESS is constructed from a PHES system, primarily for industrial parks. The REMG is composed of reheat thermal units, a photovoltaic station and a PHES system. The PHES is constructed by lower reservoirs, upper reservoirs and several MPSUs. The upper reservoirs could be built on the top of a tall building, and lower reservoirs could be placed in the basement.

Because of the power fluctuation of RE and the perturbation of load demand, frequency deviation and tie-line power interchange are inevitable for a REMG. Frequency stability reflects the balance relationship between the active power output of the generator and the load demand. Control of frequency and active power is referred to as LFC [9]. The LFC is intended to maintain the power balance in the system to ensure the frequency varies within a specified bound [10], [11].

Although some advanced controllers have been developed recently, such as fuzzy logic [12]–[14], artificial neural network [15]–[17], and distributed model predictive controller [18], the proportional integral (PI) and proportional integral derivative (PID) controllers are still the most popular

in MGs for LFC because of their simple structure and high robustness. Conventionally, PI/PID controllers employed to address the LFC issues are often tuned to enhance the stability of the power system. However, an improperly tuned PI/PID controller may exhibit poor dynamic response and may even destabilize the overall system [19]. Therefore, controllers are often optimally designed or turned by different methods, among which, artificial intelligence and heuristic-based techniques are the most attractive. Some popular meta-heuristic algorithms, e.g., the genetic algorithm (GA) [20], particle swarm optimization (PSO) [19], [21], [22], biogeography-based optimization (BBO) [23], [24], and GSA [25]–[27], have already been successfully applied and proved effective in controller optimization for the LFC problem. A powerful optimization algorithm might be decisive in handling a complex optimization problem. The problem associated with the aforementioned techniques is the fact that they may suffer from poor convergence and low exploitation. Thus, exploring a new optimization algorithm is still important to promote the control performance of the MG via controller optimization through a more robust heuristic optimization algorithm. The artificial sheep algorithm is a novel meta-heuristic optimization method based on the social behaviors of a sheep flock, which has been successfully applied in solving unit commitment problem [2], multi-objective optimization [28] and start-up strategy optimization for pumped storage unit [29]. In view of the outstanding performance of ASA, it is taken to the task of LFC problem of the REMG.

From the above discussion, we were motivated to present a new REMG with PHES and study the control strategy of LFC for the REMG. The main contributions of this paper are reflected in the following: (1) a new REMG with an ESS constructed by a specialized PHES is designed for industrial parks; (2) the LFC problem is addressed by considering different RE scenarios, system nonlinearities and operation modes of MPSU; (3) a novel heuristic algorithm has been proposed and verified for improving the optimization performance of the LFC controller.

The remaining part of this paper is organized as follows. Section II establishes a REMG with a PHES system and introduces the mathematical model of LFC. The novel meta-heuristic ASA is proposed and tested in Section III. Section IV presents case studies on the LFC problem of the REMG and discusses experimental results. Finally, the conclusions are summarized in Section V.

II. MODEL OF REMG WITH A PHES SYSTEM

A. DESCRIPTION OF THE PROPOSED MICRO-GRID SYSTEM

The micro-grid, which is part of the effective forms of distributed generation, improves the flexibility and reliability of power supply. With PHES representing most of the world's energy storage installed capacity and given its maturity and simplicity, the feasibility of a small-scale PHES is analysed by modelling each one of its components and applying it

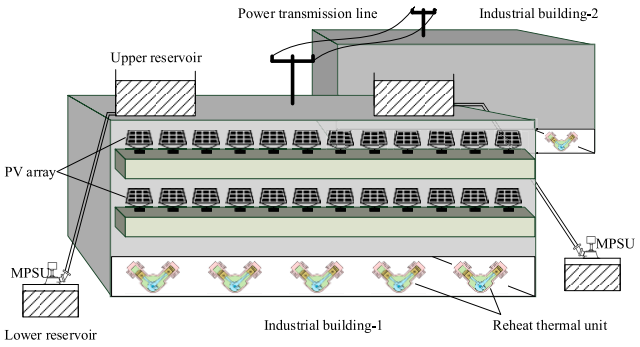

FIGURE 1. Layout of the REMG for an industrial park.

to buildings [30]. Numerous research studies have verified the application of photovoltaic systems in buildings and have considered feasibility analyses, modelling methods and control problems [31], [32]. Based on the above research studies, a REMG is constructed with photovoltaic systems, small-scale PHESs and other conventional micro-power sources. By utilizing the height of buildings, a small-scale PHES, which is composed of upper reservoirs, lower reservoirs and MPSUs, can be installed. The upper reservoirs could be built on the top of the building, and the lower reservoirs could be placed in the basement. The MPSU can operate in pump mode, and the power generated by the photovoltaic system could be stored by pumping water from the lower reservoirs to the upper. It can also operate in generating mode, and the stored energy could be released by generating electricity through the MPSU. The typical configuration of the REMG for an industrial park is illuminated shown in Fig. 1, and the micro-grid system is equipped with several reheat thermal units, a photovoltaic system with panels arranged on the surface of the buildings and a micro-scale PHES system installed in the buildings. The system consists of total 144 kW thermal units in each building, the power of each photovoltaic panel is 240W and the total power is 18kW, it is arranged on the building 1. The proposed building height is 20 meters and the pipeline flow is 0.1 cubic meters per second. The rated power of a single pumped storage unit matched with the photovoltaic system is 18kW. Two pumping storage units are installed in the building 1, and the total power is 36kW. The required reservoir capacity is

$$V = \frac{C}{P} \times Q = \frac{20\text{kW} \cdot \text{h}}{18\text{kW}} \times 0.1\text{m}^3/\text{s} \times 3600\text{s} = 400\text{m}^3.$$

So the required each upper or lower reservoir capacity is 200m^3.

B. PROBLEM FORMULATION OF THE MICRO-GRID SYSTEM WITH LFC CONTROLLER

Studies of LFC problems mainly focus on small load perturbation under the nominal operating condition of the power systems. As distributed control schemes have become increasingly popular in all types of power systems [33], a target power system is usually divided into several control areas,

each of which possesses a local controller to regulate not only the local frequency but also the tie-line load flows between the neighboring areas [34].

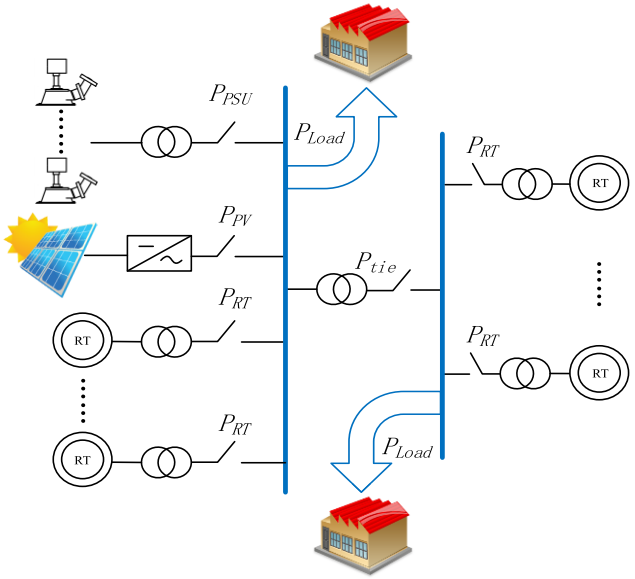

FIGURE 2. Structure of the proposed hybrid REMG.

As showed in Fig. 2, the REMG is divided into two areas. Several reheat thermal units, a photovoltaic system and MPSUs are installed on one building, named area #1, and the remaining reheat thermal units are installed in the other building, named area #2. An inverter for converting DC to AC voltage and an interconnection device (IC) are incorporated into the PV system. A circuit breaker is located between the micro-grid and the power network to provide reliable support.

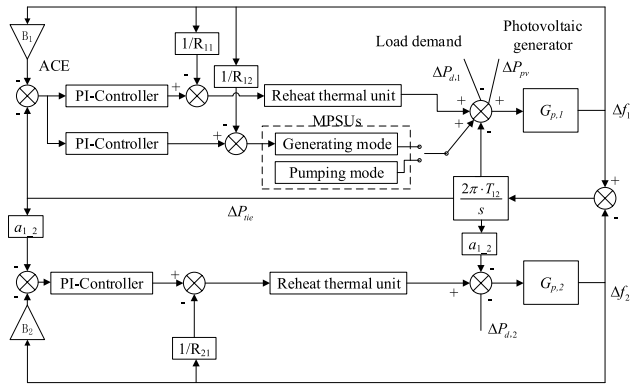

FIGURE 3. Transfer function block diagram of the industrial micro-grid power system.

The transfer function block diagram of the REMG is shown in Fig. 3, while the REMG is divided into two areas, namely, area #1 and area #2. In Fig. 3, R_{ij} is the speed regulation constant of governor, B_i is the frequency bias constant, D_i is the total damping ratio, M_i is the total machine inertia, $\mathbf{\Delta}f_i$ is the frequency deviations in each control area, $\mathbf{\Delta}P_{d,i}$ is the incremental change in system loading condition, and T_{12} is the synchronizing time constant of the tie-line. For the sake of convenience, the subscript i represents the number of the control area, taking the value of 1 or 2, the subscribe j represents the j^{th} unit in control area. K_p and K_i are the electric governor proportional and integral gains, respectively, $\mathbf{\Delta}P_{tie}$ is the tie-line power deviation and $\mathbf{\Delta}P_{pv}$ is the photovoltaic energy fluctuation.

The transfer function between the power disturbance and the frequency disturbance in power system is given as follows:

$$G_p(s) = \frac{\Delta f(s)}{\Delta P_g(s) - \Delta P_d(s)} = \frac{1}{Ms + D} \tag{1}$$

The tie-line is the electric transmission line between the interconnected areas. When ignoring line loss, the model of the tie-line load flow between area #1 and area #2 is defined as:

$$\Delta P_{tie,12} = \frac{2\pi T_{12}}{s}(\Delta f_1 - \Delta f_2) \tag{2}$$

Inputs to the PI-controllers are the area control error (ACE) of the respective areas and controlled inputs (u_1, u_2) to the plant with PI-controller structure are defined as follows:

$$\begin{cases} ACE_1 = B_1 \Delta f_1 + \Delta P_{tie,12} \\ ACE_2 = B_2 \Delta f_2 + a_{1\_2} \Delta P_{tie,12} \end{cases} \tag{3}$$

where $B_{\text{i}} = \sum_{\text{j}=1}^{Ni} \frac{1}{Rij} + D_i$ denotes the frequency regulation parameter in the area #i.

$$\begin{cases} u_1 = K_{p1} ACE_1 + K_{i1} \int ACE_1 \\ u_2 = K_{p2} ACE_2 + K_{i2} \int ACE_2 \end{cases} \tag{4}$$

ACE is treated as the controlled output of the LFC system, which is used to identify any deviation between the power generation and the load demands. In an optimal control system, the integral criterion is the most commonly used performance index in optimal control theory. The commonly used performance indices based on integral criteria are the integral square error (ISE), integral absolute error (IAE), integral time multiplies of square error (ITSE) and integral time absolute error (ITAE). The features of each performance indices are presented in [35].

C. MODEL OF THE REHEAT THERMAL UNITS

Reheat thermal unit is widely used in MG system. In this case, note that several reheat thermal units in the REMG system are treated as a whole (without explanation, the reheat thermal unit/turbine mentioned later is considered as a whole.) As shown in Fig.4, the model of reheat thermal turbine is defined as follows:

$$G_r(s) = \frac{K_r T_r s + 1}{T_r s + 1} \cdot \frac{1}{T_t s + 1} \tag{5}$$

The first half of the transfer function represents the reheat section. T_t is the turbine time constant, T_r is the reheat time constant, and K_r is the reheat gain.

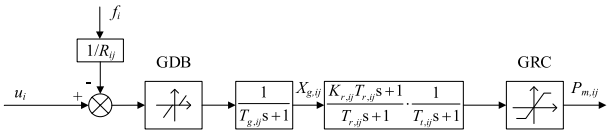

FIGURE 4. Transfer function of the reheat thermal unit.

The model of reheat thermal governor is defined as follows:

$$G_g(s) = \frac{1}{T_g s + 1} \tag{6}$$

where T_g is the governor time constant.

In Fig. 3, $X_{g,ij}$ is the opening deviation from the nominal state of the steam valve in the reheat thermal unit and $P_{m,ij}$ is the mechanical power deviation from the nominal state of the jth unit in the area #i.

The generation rate constraint (GRC) imposes a practical limit on the generation of power system, mainly because of the presence of thermal and mechanical constraints. From Fig. 4, the addition of limiters with the steam turbine is quite realistic because the electrical system power is always generated at a specified rate [36].

Another typical constraint in the LFC system, the GDB nonlinearity, is illustrated in Fig. 4. On account of the dead band, the input signal of the turbine governor would experience operational failures to avoid excessive vibrations in the vicinity of the equilibrium point [18].

D. MODEL OF THE MICRO-PUMPED STORAGE UNITS

The typical operation mode of MPSUs is always switched between pumping mode and generating mode. The transfer function frame is shown in Fig. 5.

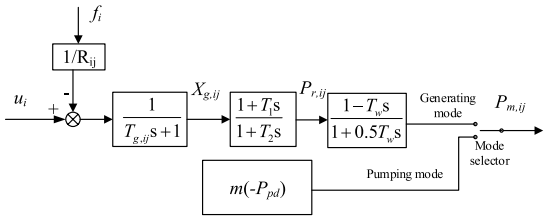

FIGURE 5. Transfer function of the micro pumped storage units.

When working on the generating mode, the MPSUs generate electricity to support the grid and maintain the frequency stability of the micro-grid system [37], [38]. Apart from the controller, the model of MPSUs is composed of three parts, namely the actuator, the transient droop compensator (TDC) and the hydraulic turbine.

The actuator executes the control law given by the controller, which amplifies and transforms the control signal to obtain adequate power to drive the turbine. The model of actuator is defined as follows:

$$G_g(s) = \frac{1}{T_g s + 1} \tag{7}$$

where T_g is the time constant. Output of this section $X_{g,ij}$ represents the opening deviation from nominal state of the guide vane, as shown in Fig. 5.

The model of hydraulic turbine is defined as follows:

$$G_t(s) = \frac{1 - T_w s}{1 + 0.5 T_w s} \tag{8}$$

where T_w is the water starting time of the hydraulic turbine. The hydraulic turbine transfer function is inherently of non-minimum phase because of the water inertia in pressure pipes, thus exhibiting unstable system dynamic responses.

A recommended solution reported in [39]–[43] was to equip the speed governor of the hydro turbine with a TDC to ensure its stability. The transfer function of the compensator is defined as below:

$$G_c(s) = \frac{1 + T_1 s}{1 + T_2 s} \tag{9}$$

where the compensator parameters $T_1 = T_R, T_2 = (R_T/R_{12}) \cdot T_R$ and the empirical formulae for the parameter tuning of the reset time T_R and transient droop coefficient R_T are defined as follows [39]:

$$\begin{cases} R_T = [2.3 - 0.15\,(T_w - 1.0)] \cdot T_w/M \\ T_R = [5 - 0.50\,(T_w - 1.0)] \cdot T_w \end{cases} \tag{10}$$

where M represents the machine inertia. In addition, $P_{r,ij}$ denotes the output of the compensator in Fig. 5.

When working on the pumping mode, MPSUs could be seen as pumps, which consume the PV energy by pumping water from the lower reservoir to the upper reservoir. Frequency stability of the REMG is affecting the operation of MPSUs in pumping mode. By controlling the starting number of pumps, the power balance between load demand and power output of the REMG could be adjusted.

The schematic of the water pump control mode is illustrated in Fig. 5. $m = \{1, 2, \ldots, n\}$, where m is the number of units that will stop, n is the total number of units in pumping mode, and $-P_{pd}$ is the rated pumping power of a unit. The output mechanical power deviation of MPSUs is presented as $P_{m,ij}$.

III. LFC CONTROLLER OPTIMIZATION FOR THE REMG SYSTEM USING ASA

A. THEORETICAL KNOWLEDGE OF ASA

Consider a sheep flock with N sheep, the position of the ith sheep at specific time 't' is defined as:

$$\mathbf{X}_i(t) = (x_i^1(t), \ldots, x_i^d(t), .., x_i^D(t)) \quad \text{for} \quad i = 1, 2, \ldots, N \tag{11}$$

where x_i^d represents the position of ith sheep in the dth dimension, D is the dimension of the position.

The optimization involves solving the following minimization problem:

$$\begin{cases} \min\ f\ (\mathbf{X}_i) \\ s.t.\ x_i^d \in [b_l^d, b_u^d], \quad d = 1, \ldots, D \end{cases} \tag{12}$$

where $\mathbf{B}_L = (b_l^1, \ldots, b_l^d, \ldots, b_l^D)$ is the lower boundary of the searing space, and $\mathbf{B}_U = (b_u^1, \ldots, b_u^d, \ldots, b_u^D)$ is the upper boundary of the searing space. The objective function value of the ith agent at time 't' is expressed as $F_i^t = f(\mathbf{X}_i(t))$.

1) LEADING OF THE BELLWETHER

The influence of the bellwether is decisive. When the bellwether moves with a large stride, an individual will adjust its motion trajectory to follow the bellwether closely. The position of the bellwether should be recorded and inherited; this position is denoted as $X^B(t) = [X_d^B(t)]_{1\times D}$. The influence of the bellwether acting on the ith sheep is expressed as the bellwether vector, denoted by $\mathbf{X}_i^{bw}(t) = \left[x_{i,d}^{bw}(t)\right]_{1\times D}$.

The bellwether vector that affects the movement of the ith agent, $i = 1, \ldots, N$, is defined as:

$$\begin{cases} x_{i,d}^{bw}(t) = x_d^B(t) + c_2 \cdot \delta_{i,d} \\ \delta_{i,d} = \left| c_1 \cdot x_d^B(t) - x_{i,d}(t) \right| \end{cases} \tag{13}$$

where $\delta_{i,d}$ is the influence scope of the bellwether playing on the ith sheep on the dth dimension, $c_1 = 1 + (1-\alpha) \cdot rand_1$, $c_2 = 2w \cdot rand_1$, α is the coefficient of leading scope, $rand_1$ is a random number generated in $[-1, 1]$, and$w$ is a dynamic weight that linearly decreases from 1 to 0 over the course of iterations.

The coefficient c_1 is a random value whose centre is 1 and whose radius is determined by parameter α, which is selected from [0, 1]. α is a control parameter, that influences the consensus effect of the bellwether in defining the distance vector. When α tends to 1, the consensus influence of the bellwether is emphasized; when α tends to 0, the stochastic components are enhanced. The coefficient c_2 is a random dynamic number that is automatically generated, and its random range is linearly decreased over the course of iterations.

2) INDIVIDUAL STROLLING

Every individual of the flock forages autonomously in a local area; this behavior is called "self-awareness". The mathematical model of "individual strolling" to represent self-awareness of an individual sheep in the process of foraging is proposed as follows. We define a location vector $\mathbf{X}_i^{self}(t) = \left[x_{i,d}^{self}(t)\right]_{1\times D}$ to denote self-awareness in foraging.

The self-awareness vector that affects the movement of the ith agent, $i = 1, \ldots, N$, is defined as:

$$\begin{cases} x_{i,d}^{self}(t) = x_{i,d}(t) + rand_2 \cdot \varepsilon_{i,d} \\ \varepsilon_{i,d} = e^{-\beta \cdot rand_1} \cdot \cos(2\pi \cdot rand_1) \cdot \delta_{i,d} \end{cases} \tag{14}$$

where $rand_2$ is a random number generated from [0, 1], and the term $cos\,(2\pi \cdot rand_1)$ is used to generate periodic random motion.

The vector $X_{i,d}^{self}$ represents the self-driven behavior and local random search of a sheep; this search consists of a series of nonlinear operations. The β parameter is a positive number that modulates the amplitude of the strolling step. As β increases, the sheep's jump steps increase exponentially and vice versa. As a result, this parameter controls the resolution of individual exploration. The value of β should be chosen according to the search scope of the optimization problem.

In a sheep flock, the direction of the sheep flock is determined by following the lead of the bellwether and autonomous foraging. Based on the discussion above, the movement of a sheep is affected by its self-awareness and the summoning of the bellwether. The individuals in the artificial sheep flock will automatically update their positions as follows:

$$\begin{cases} x_{i,d}(t+1) = \varphi_i \cdot x_{i,d}^{self}(t) + (1-\varphi_i) \cdot x_{i,d}^{bw}(t) \\ \varphi_i = w \cdot rand_2 \end{cases} \tag{15}$$

where w is linearly decreased from 1 to 0 over the course of iterations and r_3 is random number generated in [0, 1].

3) COMPETITION STRATEGY

In ASA, competition mechanism is designed to maintain the diversity of the flock. For the minimization problem, at a specific time 't', calculate the average value of N objective function values of the flock F_{ave}^t and the minimal objective function value $F_{\min}^t$.

For the ith sheep, if the elimination criteria below is satisfied:

$$F_i^t > F_{ave}^t \tag{16}$$

then, the ith sheep $\mathbf{X}_i$ is eliminated and reinitialized between $[\mathbf{B}_L, \mathbf{B}_U]$.

B. LFC CONTROLLER OPTIMIZATION PROCEDURES USING ASA

In the proposed method, the ASA is used to optimize the LFC control parameters of the REMG. The steps are described as follows:

Step 1: Build the simulation platform of the aforementioned micro-grid and set up the system parameters;

Step 2: Select the objective function. The ITAE based objective function is applied to tune the controller parameters using the ASA algorithm. The fitness function or objective function (J) is defined as:

$$J = \int_0^{T_{total}} t \cdot [(|\Delta f_1|) + (|\Delta f_2|)]dt \tag{17}$$

where T_{total} is the total simulation time. The gains of K_p and K_i of each PI-controller are the optimization variables.

The PI controller parameters are subjected to the constraints of boundaries:

$$\begin{cases} K_{p,\min} \le K_{p,j} \le K_{p,\max} \\ K_{i,\min} \le K_{i,j} \le K_{i,\max} \end{cases}$$

where $K_{pi,min}$ and $K_{pi,max}$ are the minimum and maximum values of the PI-controller parameters respectively; j is the number of controllers, where $j = 1$ or 2 for the proposed REMG.

Step 3: Initialization. Initialize locations $\mathbf{X}_i(0)$ of the sheep flock with N sheep in the solution space with boundaries $[\mathbf{B}_L, \mathbf{B}_U]$, set the first sheep as the bellwether $\mathbf{X}_B = \mathbf{X}_1(0)$, $J_B = J_1^0$; set the other control parameters: the initial scope coefficient of leading α and the modulation coefficient of strolling β; set the total number of iteration T, and the current number of iteration $t = 0$.

Step 4: Objective function calculation. For the ith $(i = 1, .., N)$ agent, the fitness J_i^t is calculated as follows:

Step 4.1: Decode the agent's position X_i, and obtain the control parameters $K_{p,j}$ and $K_{i,j}$ of each controller.

Step 4.2: Set the following parameters for the micro-grid system and start the established simulation platform; sample and record system outputs including the frequency deviation f_i.

Step 4.3: Calculate the objective function Eq. (17) and let $J_i^t = J_{ITAE}$.

Step 5: Calculate the bellwether vector, self-awareness vector and then update the position of the flock, according to the instructions in Section 3.

Step 6: Set, t = t + 1; if t > T, then stop the simulation and output the bellwether's position as the final solution; else, go to Step 4.

IV. EXPERIMENTS AND ANALYSIS OF THE RESULTS

Experiments are designed to verify the feasibility of using PHES as ESS in a REMG and to confirm the effectiveness of LFC controller optimization. All the simulations are executed on a personal computer Core i7, 2.00 GHz, 8 GB RAM, utilizing the Windows 10 operating system. The simulation platform is MATLAB R2014a.

The nominal values of system parameters are taken from [18] and presented in the Appendix. For all experiments, the reheat thermal unit includes nonlinear sections, e.g., GRC and GDB, and the value of GDB is specified to be 0.05% and the thermal system is considered with GRC of 0.01 p.u. /sec.

The LFC control parameters of the REMG are optimized by applying ASA. In the following experiments, the parameters of ASA are set as: the initial scope coefficient of leading $\alpha = 2$ and the modulation coefficient of strolling $\beta = 1$, the population size is 30, and the total number of iteration $T = 300$. The boundaries of PI controller parameters $[K_{pi,min}, K_{pi,max}]$ are selected between [0, 5].

Because the photovoltaic power will fluctuate with regard to the change of weather and sun condition in different seasons, the photovoltaic energy fluctuation ΔP_{pv} is simulated in different scenarios, as shown in Fig. 6; the data was collected from solar radiation data in Aberdeen [44].

A. LFC PERFORMANCE OF DIFFERENT SCENARIOS

In this part, multi-step load perturbation is considered in the micro-grid. The MPSUs are operating in generating mode to testify the excellent performance in frequency regulation. The step changes of the load demand in the interval of 90 seconds are demonstrated in Fig. 7. Photovoltaic power fluctuation ΔP_{pv} can be considered as a negative load demand. By adding

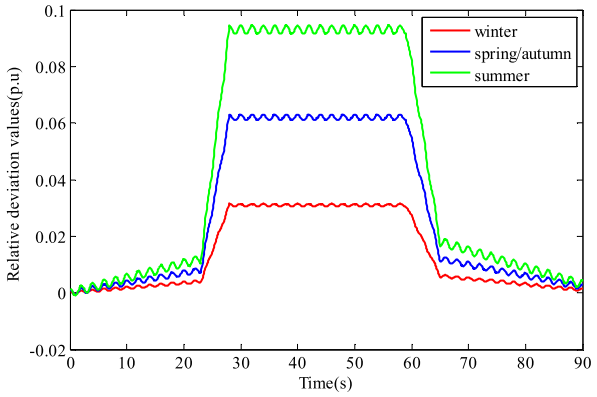

FIGURE 6. Photovoltaic power fluctuation scenarios in different seasons.

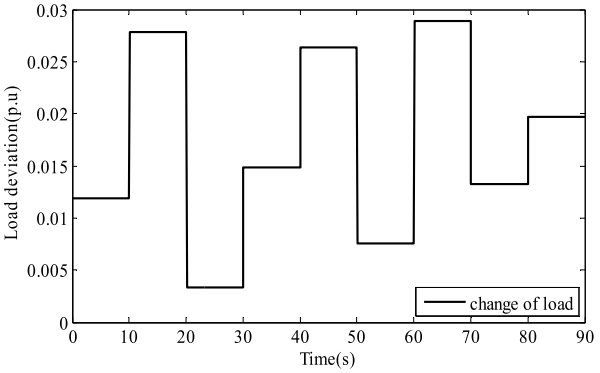

FIGURE 7. Step changes of the load in the interval of 90s.

PV to the original load, the equivalent load deviations in different scenarios are illustrated in Fig. 8. The fluctuation of the equivalent load will excite strong disturbance to the two-area REMG, and the LFC performance will be verified.

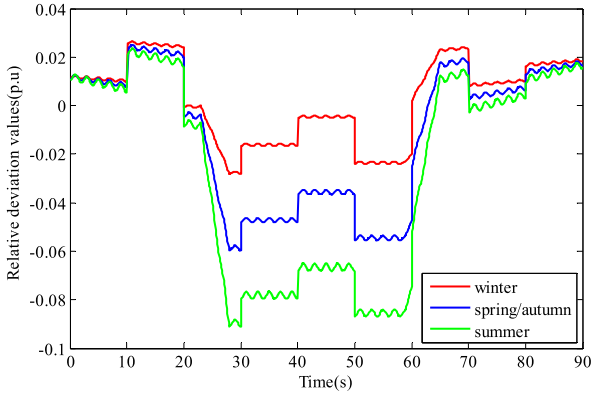

FIGURE 8. Equivalent load deviations in different scenarios.

To demonstrate the performance of the REMG system, three different scenarios of photovoltaic power fluctuations are studied. The PI-controllers are employed in each control area and its gains are optimally searched by the ASA. The equivalent load deviation is given to area #1 and multi-step load perturbation is given to area #2 for identifying

the dynamic stability of the whole micro-grid system. The equivalent load deviation in winter is the smallest, i.e., only a slight impact on the system occurs in winter, making it easy to guarantee the frequency stability and power balance. In contrast, the scenario in summer is hard difficult for the load frequency control.

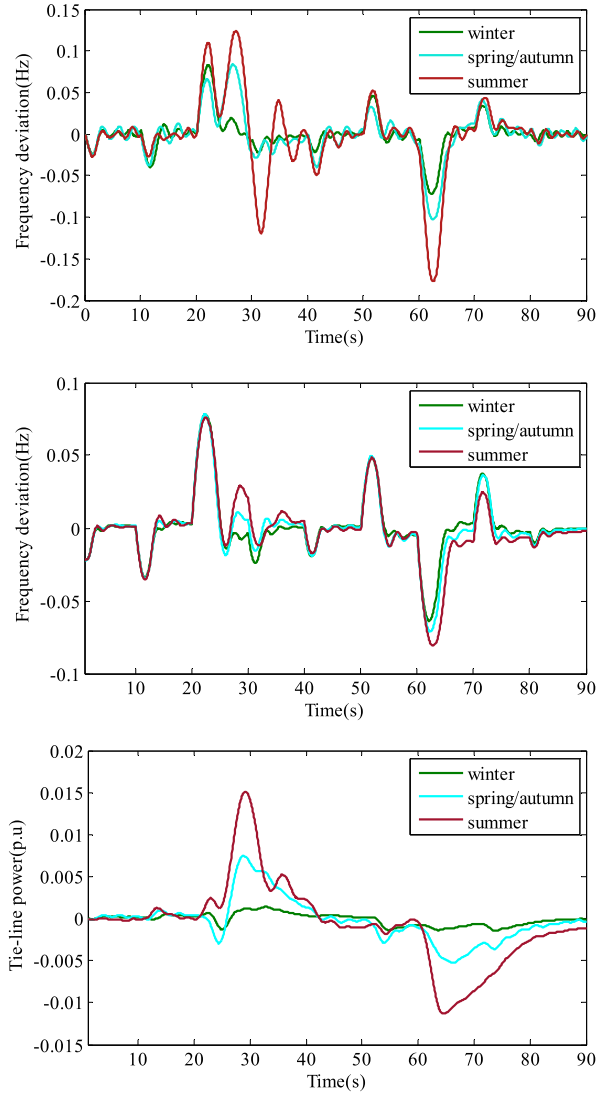

FIGURE 9. Dynamic performance of micro-grid power system in different scenarios.

The optimal values of controller's gains, minimum fitness values, and maximum tie-line power flow with ASA including GRC and GDB are listed in Table 1. The simulation results of the dynamic of system frequencies of each area and tie-line load flows are shown in Fig. 9 in different scenarios. Taken altogether, all the indices satisfy the control requirements. The ITAE value and maximum deviations of Δf_1, Δf_2 and ΔP_{tie} are increased with the change of photovoltaic energy fluctuation in different seasons. It can also be demonstrated that ASA-tuned PI-controllers are robust and performed satisfactorily with the application of multiple load perturbation. The maximum step perturbation of equivalent load is between 60 second and 65 second, and the ASA-tuned PI-controllers effectively control excessive frequency fluctuation of the REMG with a second level settling time.

TABLE 1. Optimal value of controller gain, performance indices of system oscillations in different scenarios.

Season	PI-controller gains					
	$K_{P1,1}$	$K_{i1,1}$	$K_{p1,2}$	$K_{i1,2}$	K_{p2}	K_{i2}
Winter	4.80	2.06	1.06	0.74	4.96	2.64
Spring/autumn	4.52	1.90	1.99	0.44	4.16	2.44
Summer	3.83	0.15	2.20	1.17	4.45	2.83
Season	ITAE value	Maximum deviation				
		Δf_1	Δf_2	ΔP_{tie}		
Winter	16.8369	0.0828	0.0784	0.0015		
Spring/autumn	22.5629	0.1029	0.0784	0.0075		
Summer	30.4263	0.1778	0.0810	0.0151		

B. PUMPING EFFECT ANALYSIS

In this part, the frequency stability and power balance of the REMG is studied when the MPSUs operate in pumping mode. When operating in pumping mode, the MPSUs consume the redundant PV power, causing the equivalent load to vary slightly. In this situation, the controllers would adjust the power output of reheat thermal units to respond the fluctuation of power and load after the compensation of the MPSUs. To show the compensation effect of MPSUs, the LFC problems with and without the MPSUs are studied.

TABLE 2. Optimal value of the controller gain and performance indices of system oscillations with or without pumping storage units.

Unit type	PI-controller gains			
	$K_{p1,1}$	$K_{i1,1}$	$K_{p1,2}$	$K_{i1,2}$
Only reheat thermal units	3.90	3.15	1.10	0.92
With MPSUs	3.90	3.15	1.10	0.92
Unit type	ITAE value	Maximum deviation		
		Δf_1	Δf_2	ΔP_{tie}
Only reheat thermal units	0.3606	0.0309	0.0063	0.0022
With MPSUs	0.2350	0.0249	0.0042	0.0015

To validate the compensation performance, a +15% step load perturbation (SLP) in area #1 is simultaneously imposed on the micro-grid power system at $t = 10$ s simultaneously. The dynamic response of system frequencies of each area and tie-line load flows is shown in Fig. 10. The optimal values of the controller's gains, the minimum fitness values, and the tie-line power flow are illustrated in Table 2. It is remarkable that faster frequency regulation and smaller frequency deviation are obtained by considering MPSUs. Benefiting from the compensation effect of MPSUs on power fluctuation,

the frequency stability indices are all reduced significantly, with decreasing amplitude of 19.42% (Δf_1), 33.33% (Δf_2) and 31.82% (ΔP_{tie}).

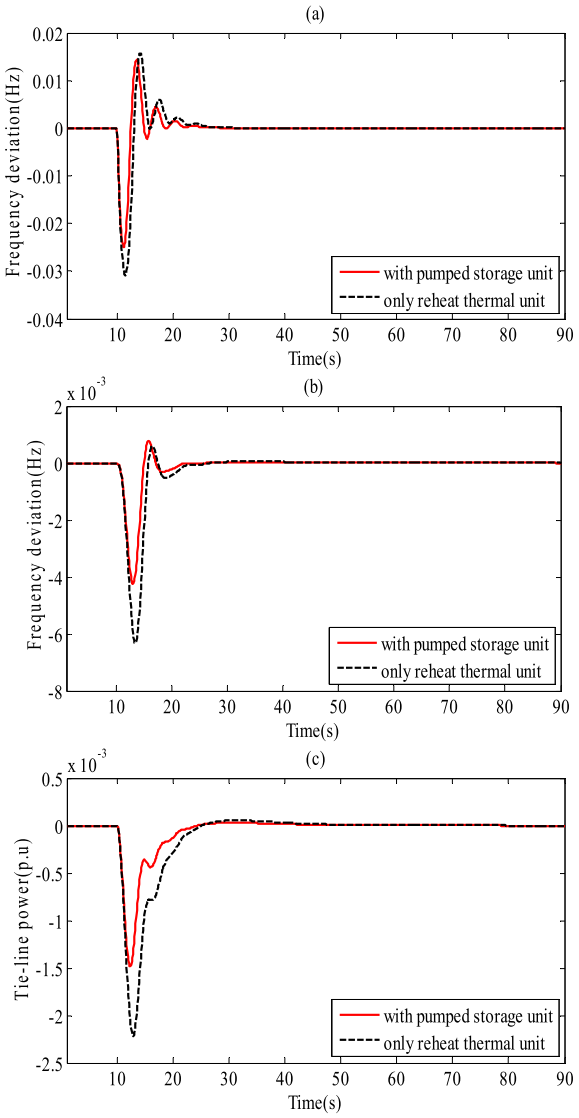

FIGURE 10. Comparative deviation results of micro-grid system with or without pumping storage units.

From Fig. 10 and Table 2, it is evident that MPSUs play an important role of power compensation in the system for the frequency regulation. The dynamic characteristics of the tie-line flow are also improved significantly.

C. SENSITIVITY ANALYSIS

To illustrate the robustness of the designed controllers, a sensitivity analysis is performed by varying the operating loading condition and the system parameters. In this subsection, MPSUs operate in generating mode. System parameters such as T_r and T_g are varied in the range of ±50% in steps of 25%. The performance of LFC of the REMG is evaluated with the optimal controller values obtained at the nominal operating condition. The spring/autumn equivalent load deviation is injected to area #1, and the multi-step load perturbation is injected to area #2; the optimal PI-controller gains are those shown in **Table 1**.

TABLE 3. Sensitivity analysis of the micro-grid system with ASA.

Parameter	% of change	ITAE value	Maximum deviation $\triangle f_1$	$\triangle f_2$	$\triangle P_{tie}$
Nominal	0	22.5629	0.1029	0.0784	0.0075
T_g	+50	26.7459	0.0933	0.0722	0.0085
	+25	28.0459	0.1636	0.0771	0.0110
	-25	26.3069	0.1455	0.0782	0.0090
	-50	25.3782	0.1438	0.0779	0.0088
T_t	+50	41.3506	0.1915	0.0959	0.0151
	+25	27.6894	0.0996	0.0740	0.0081
	-25	23.6211	0.1214	0.0786	0.0078
	-50	22.1496	0.1212	0.0763	0.0073
T_r	+50	27.6062	0.1535	0.0787	0.0098
	+25	26.7838	0.1559	0.0789	0.0102
	-25	27.7306	0.1510	0.0801	0.0090
	-50	27.2010	0.1632	0.0714	0.0106
K_r	+50	27.4818	0.1550	0.0830	0.0094
	+25	27.3078	0.1528	0.0760	0.0098
	-25	29.4359	0.1606	0.0773	0.0108
	-50	39.6363	0.1734	0.0847	0.0112
R	+50	27.0174	0.1493	0.0807	0.0104
	+25	27.0226	0.1447	0.0812	0.0091
	-25	28.0913	0.1694	0.0755	0.0108
	-50	83.1708	0.1944	0.1443	0.0143
M	+50	19.5949	0.1060	0.0539	0.0079
	+25	22.0335	0.1259	0.0646	0.0083
	-25	34.0557	0.1824	0.0996	0.0121
	-50	46.4621	0.1962	0.1521	0.0119
D	+50	24.8762	0.1346	0.0751	0.0080
	+25	23.4153	0.1123	0.0769	0.0077
	-25	24.4070	0.1232	0.0800	0.0076
	-50	28.5982	0.1560	0.0835	0.0093
T_w	+50	30.3357	0.1337	0.0788	0.0104
	+25	25.6846	0.1158	0.0785	0.0078
	-25	22.9701	0.0988	0.0761	0.0083
	-50	19.9092	0.0903	0.0759	0.0049

The control performances with parametric variation are presented in **Table 3**, from which, it is demonstrated that fitness value and maximum deviation of frequency and tie-line power oscillations for system parameter variations are within the acceptable limit and the frequency deviations of all test are less than 0.2Hz.

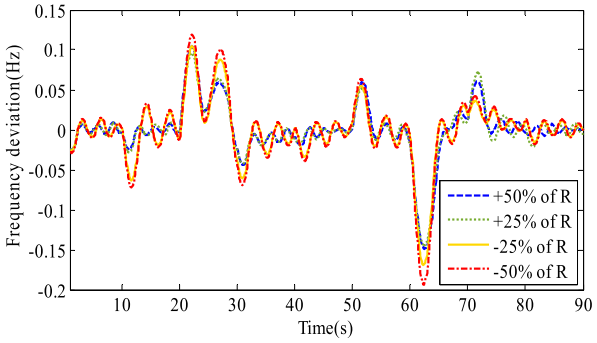

FIGURE 11. Sensitivity analysis of the micro-grid system under the variation of R(frequency deviation in area #1).

The selected dynamic responses of the frequency deviation in area #1 are shown to highlight the impact of system

parameter variation straightway; the dynamic responses with R and M varying are shown in Figs. 11 and Figs. 12 respectively.

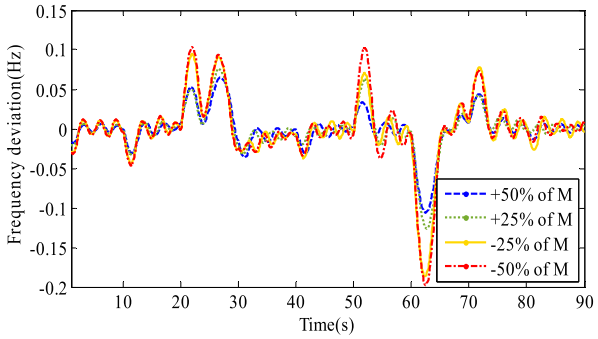

FIGURE 12. Sensitivity analysis of the micro-grid system under the variation of M(frequency deviation in area #1).

Note that the speed regulation constant of governor R and the total machine inertia M have a certain influence on the dynamic stability of the system. The frequency deviation indices increase gradually as the variation of system parameter; however, the maximum deviation frequency in area #1 is still lower than 0.2Hz. From the results of this part, it could be concluded that proposed ASA-tuned PI-controllers are robust to fulfil a stable control of the REMG when some system parameters change.

V. CONCLUSIONS

Renewable energy integrated micro grid with a PHES system adopting the ESS and the LFC problem of the REMG were studied. In this study, the REMG is composed of reheat thermal units and photovoltaic power system and MPSUs. To improve the control performance of LFC of the proposed REMG, a novel meta-heuristic optimization algorithm named ASA was adopted to tune the controller parameters before verification based on benchmark functions. The experiments of load and frequency control were conducted using a simulated REMG model on the MATLAB platform, and the impacts on different PV scenarios, different working mode of MPSUs and system parameter variations were studied.

The comparison results on benchmark functions proved that the ASA shows advantages regarding both convergence speed and global optimization ability. In particular, ASA was found to have a very good performance regarding high dimensional test functions.

The results of LFC experiments showed that the MPSUs in generating mode can cooperate with reheat thermal units to regulate frequency stability. Under the control of the optimized controller, the REMG was found to exhibit excellent dynamic stability. When MPSUs are working in pumping mode, these units could consume redundant PV power and compensate the fluctuations of the power output and the load demand. In this situation, control performances of the REMG were found to be excellent with acceptable frequency deviation indices. Finally, the results of the sensitivity analysis demonstrated that the ASA tuned PI-controllers can guarantee a satisfactory control performance under uncertainty of system parameter variation. Although the feasibility of the REMG with PHES and the performance of the controller optimization were verified, some intelligent controllers and more flexible operation of MPSUs are worthystudy in the future.

TABLE 4. System parameters.

Symbol	Value	Symbol	Value
$T_{g,11}$ (sec)	0.08	$T_{g,21}$ (sec)	0.08
$T_{r,11}$ (sec)	10	$T_{r,21}$ (sec)	10
$K_{r,11}$	0.5	$K_{r,21}$	0.5
$T_{t,11}$ (sec)	0.4	$T_{t,21}$ (sec)	0.4
R_{11} (pu/pu)	0.05	R_{21} (pu/pu)	0.05
$T_{g,12}$ (sec)	0.15	M_2(sec/pu)	20
$T_{w,12}$ (sec)	1	D_2 (pu/pu)	1
R_{12} (pu/pu)	0.05	a_{1_2}	-0.8
M_1 (sec/pu)	20	T_{12} (pu/Hz)	0.25
D_1 (pu/pu)	1	f(Hz)	50

APPENDIX

See Table 4.

REFERENCES

[1] H. Quan, D. Srinivasan, and A. Khosravi, "Integration of renewable generation uncertainties into stochastic unit commitment considering reserve and risk: A comparative study," *Energy*, vol. 103, pp. 735–745, May 2016.
[2] W. Wang, C. Li, X. Liao, and H. Qin, "Study on unit commitment problem considering pumped storage and renewable energy via a novel binary artificial sheep algorithm," *Appl. Energy*, vol. 187, pp. 612–626, Feb. 2017.
[3] E. Reihani, S. Sepasi, L. R. Roose, and M. Matsuura, "Energy management at the distribution grid using a Battery Energy Storage System (BESS)," *Int. J. Elect. Power Energy Syst.*, vol. 77, pp. 337–344, May 2016.
[4] X. Luo, J. Wang, M. Dooner, and J. Clarke, "Overview of current development in electrical energy storage technologies and the application potential in power system operation," *Appl. Energy*, vol. 137, pp. 511–536, Jan. 2015.
[5] M. Z. Daud, A. Mohamed, and M. A. Hannan, "An improved control method of battery energy storage system for hourly dispatch of photovoltaic power sources," *Energy Convers. Manag.*, vol. 73, pp. 256–270, Sep. 2013.
[6] G. Boukettaya and L. Krichen, "A dynamic power management strategy of a grid connected hybrid generation system using wind, photovoltaic and Flywheel Energy Storage System in residential applications," *Energy*, vol. 71, pp. 148–159, Jul. 2014.
[7] T. Ma, H. Yang, L. Lu, and J. Peng, "Technical feasibility study on a standalone hybrid solar-wind system with pumped hydro storage for a remote island in Hong Kong," *Renew. Energy*, vol. 69, pp. 7–15, Sep. 2014.
[8] M. H. Khooban, T. Niknam, F. Blaabjerg, and T. Dragičević, "A new load frequency control strategy for micro-grids with considering electrical vehicles," *Electr. Power Syst. Res.*, vol. 143, pp. 585–598, Feb. 2017.
[9] D. Guha, P. K. Roy, and S. Banerjee, "Quasi-oppositional differential search algorithm applied to load frequency control," *Eng. Sci. Technol., Int. J.*, vol. 19, no. 4, pp. 1635–1654, 2016.
[10] H. Bevrani, F. Habibi, P. Babahajyani, M. Watanabe, and Y. Mitani, "Intelligent frequency control in an AC microgrid: Online PSO-based fuzzy tuning approach," *IEEE Trans. Smart Grid*, vol. 3, no. 4, pp. 1935–1944, Dec. 2012.
[11] J. Yang *et al.*, "Load frequency control in isolated micro-grids with electrical vehicles based on multivariable generalized predictive theory," *Energies*, vol. 8, no. 3, pp. 2145–2164, 2015.
[12] V. Chandrakala, B. Sukumar, and K. Sankaranarayanan, "Load frequency control of multi-source multi-area hydro thermal system using flexible alternating current transmission system devices," *Electr. Power Compon. Syst.*, vol. 42, no. 9, pp. 927–934, 2014.

[13] H. Yousef, "Adaptive fuzzy logic load frequency control of multi-area power system," *Int. J. Elect. Power Energy Syst.*, vol. 68, pp. 384–395, Jun. 2015.
[14] C. Li, Y. Mao, J. Zhou, N. Zhang, and X. An, "Design of a fuzzy-PID controller for a nonlinear hydraulic turbine governing system by using a novel gravitational search algorithm based on Cauchy mutation and mass weighting," *Appl. Soft Comput.*, vol. 52, pp. 290–305, Mar. 2017.
[15] S. Prakash and S. K. Sinha, "Neuro-fuzzy computational technique to control load frequency in hydro-thermal interconnected power system," *J. Inst. Eng. India B*, vol. 96, pp. 273–282, Sep. 2014.
[16] B. Singh and S. Sharma, "Neural network based voltage and frequency controller for isolated wind power generation," *IETE J. Res.*, vol. 57, no. 5, pp. 467–477, 2011.
[17] S. Prakash and S. K. Sinha, "Simulation based neuro-fuzzy hybrid intelligent PI control approach in four-area load frequency control of interconnected power system," *Appl. Soft Comput.*, vol. 23, pp. 152–164, Oct. 2014.
[18] Y. Zheng, J. Zhou, Y. Xu, Y. Zhang, and Z. Qian, "A distributed model predictive control based load frequency control scheme for multi-area interconnected power system using discrete-time Laguerre functions," *ISA Trans.*, vol. 68, pp. 127–140, May 2017.
[19] S. S. Dhillon, J. S. Lather, and S. Marwaha, "Multi objective load frequency control using hybrid bacterial foraging and particle swarm optimized PI controller," *Int. J. Elect. Power Energy Syst.*, vol. 79, pp. 196–209, Jul. 2016.
[20] F. Daneshfar and H. Bevrani, "Multiobjective design of load frequency control using genetic algorithms," *Int. J. Elect. Power Energy Syst.*, vol. 42, no. 1, pp. 257–263, 2012.
[21] S. S. Dhillon, J. S. Lather, and S. Marwaha, "Multi area load frequency control using particle swarm optimization and fuzzy rules," *Procedia Comput. Sci.*, vol. 57, pp. 460–472, Mar. 2015.
[22] N. H. Saad, A. A. El-Sattar, and A. E.-A. M. Mansour, "A novel control strategy for grid connected hybrid renewable energy systems using improved particle swarm optimization," *Ain Shams Eng. J.*, May 2017. [Online]. Available: https://doi.org/10.1016/j.asej.2017.03.009
[23] D. Guha, P. K. Roy, and S. Banerjee, "Study of dynamic responses of an interconnected two-area all thermal power system with governor and boiler nonlinearities using BBO," in *Proc. 3rd Int. Conf. Comput., Commun., Control Inf. Technol.*, 2015, pp. 1–6.
[24] D. Guha, P. K. Roy, and S. Banerjee, "Optimal design of superconducting magnetic energy storage based multi-area hydro-thermal system using biogeography based optimization," in *Proc. Int. Conf. Emerg. Appl. Inf. Technol.*, 2014, pp. 52–57.
[25] R. K. Sahu, S. Panda, and S. Padhan, "Optimal gravitational search algorithm for automatic generation control of interconnected power systems," *Ain Shams Eng. J.*, vol. 5, no. 3, pp. 721–733, 2014.
[26] R. K. Sahu, S. Panda, and S. Padhan, "A novel hybrid gravitational search and pattern search algorithm for load frequency control of nonlinear power system," *Appl. Soft Comput.*, vol. 29, pp. 310–327, Apr. 2015.
[27] C. Li, Z. Xiao, X. Xia, W. Zou, and C. Zhang, "A hybrid model based on synchronous optimisation for multi-step short-term wind speed forecasting," *Appl. Energy*, vol. 215, pp. 131–144, Apr. 2018. [Online]. Available: https://doi.org/10.1016/j.apenergy.2018.01.094
[28] X. Lai, C. Li, and J. Zhou, "A multi-objective artificial sheep algorithm," *Neural Comput Appl.*, pp. 1–35, Jan. 2018. [Online]. Available: https://doi.org/10.1007/s00521-018-3348-x
[29] Z. Wang, C. Li, X. Lai, N. Zhang, Y. Xu, and J. Hou, "An integrated start-up method for pumped storage units based on a novel artificial sheep algorithm," *Energies*, vol. 11, no. 1, p. 151, 2018, doi: 10.3390/en11010151.
[30] G. de Oliveira e Silva and P. Hendrick, "Pumped hydro energy storage in buildings," *Appl. Energy*, vol. 179, pp. 1242–1250, Oct. 2016.
[31] Y. B. Assoa, F. Sauzedde, B. Boillot, and S. Boddaert, "Development of a building integrated solar photovoltaic/thermal hybrid drying system," *Energy*, vol. 128, pp. 755–767, Jun. 2017.
[32] J. Oh, C. Koo, T. Hong, K. Jeong, and M. Lee, "An economic impact analysis of residential progressive electricity tariffs in implementing the building-integrated photovoltaic blind using an advanced finite element model," *Appl. Energy*, vol. 202, pp. 259–274, Sep. 2017.
[33] R. M. Hermans *et al.*, "Assessment of non-centralised model predictive control techniques for electrical power networks," *Int. J. Control*, vol. 85, no. 8, pp. 1162–1177, 2012.
[34] D. P. Iracleous and A. T. Alexandridis, "A multi-task automatic generation control for power regulation," *Electr. Power Syst. Res.*, vol. 73, no. 3, pp. 275–285, 2005.
[35] G. A. Hassaan, "Tuning of a novel third-order feedforward compensator; Part I: Used with underdamped second-order-like process," *Int. J. Sci. Res. Technol.*, vol. 4, no. 5, pp. 441–445, 2015.
[36] P. Kundur, N. J. Balu, and M. G. Lauby, *Power System Stability and Control*. New York, NY, USA: McGraw-Hill, 1994.
[37] C. Li, Y. Mao, J. Yang, Z. Wang, and Y. Xu, "A nonlinear generalized predictive control for pumped storage unit," *Renew. Energy*, vol. 114, pp. 945–959, Dec. 2017.
[38] C. Li, N. Zhang, X. Lai, J. Zhou, and Y. Xu, "Design of a fractional-order PID controller for a pumped storage unit using a gravitational search algorithm based on the Cauchy and Gaussian mutation," *Inf. Sci.*, vol. 396, pp. 162–181, Aug. 2017.
[39] M. Parida and J. Nanda, "Automatic generation control of a hydro-thermal system in deregulated environment," in *Proc. 8th Int. Conf. Elect. Mach. Syst.*, vol. 2. 2006, pp. 942–947.
[40] A. Khodabakhshian and R. Hooshmand, "A new PID controller design for automatic generation control of hydro power systems," *Int. J. Elect. Power Energy Syst.*, vol. 32, no. 5, pp. 375–382, 2010.
[41] R. J. Abraham, D. Das, and A. Patra, "AGC of a hydrothermal system with SMES unit," in *Proc. GCC Conf.*, 2006, pp. 1–7.
[42] E. J. Oliveira, L. M. Honório, A. H. Anzai, L. W. Oliveira, and E. B. Costa, "Optimal transient droop compensator and PID tuning for load frequency control in hydro power systems," *Int. J. Elect. Power Energy Syst.*, vol. 68, pp. 345–355, Jun. 2015.
[43] J. Kennedy and R. C. Eberhart, "Particle swarm optimization," in *Proc. IEEE Int. Conf. Neural Netw.*, 1995, pp. 1942–1948.
[44] M.-H. Khooban, T. Niknam, F. Blaabjerg, P. Davari, and T. Dragicevic, "A robust adaptive load frequency control for micro-grids," *ISA Trans.*, vol. 65, pp. 220–229, Nov. 2016.

YANHE XU received the B.S. degree in water conservancy and hydropower engineering from the Xi'an University of Technology in 2012 and the Ph.D. degree in hydraulic engineering from the Huazhong University of Science and Technology (HUST) in 2017. He is currently a Lecturer with the School of Hydropower and Information Engineering, HUST. His research interest includes control and fault diagnosis of hydroelectric units.

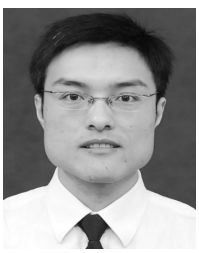

CHAOSHUN LI (M'13) received the B.S. degree in thermal energy and power engineering from Wuhan University, Wuhan, China, in 2005, and the Ph.D. degree in water conservancy and hydropower engineering from the Huazhong University of Science and Technology (HUST) in 2010. He is currently a Professor with the School of Hydropower and Information Engineering, HUST. His research interests include pumped storage units, and the configuration, scheduling and control of microgrids.

ZANBIN WANG received the B.S. degree in water conservancy and hydropower engineering from the Huazhong University of Science and Technology in 2015, where he is currently pursuing the M.S. degree in water conservancy and hydropower engineering. His research interests include modeling and control of pumped storage and microgrids.

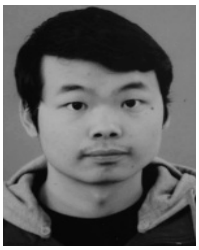

NAN ZHANG received the B.S. degree in electronic information engineering from Wuhan Textile University, Wuhan, China, in 2014. He is currently pursuing the Ph.D. degree in water conservancy and hydropower engineering at the Huazhong University of Science and Technology. His research interests include control theory, system identification and modeling of power generation system.

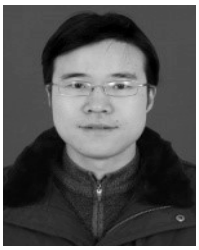

BING PENG received the Ph.D. degree in hydraulic and electric engineering from the Huazhong University of Science and Technology. His research interests include automation of hydropower plants.